Enhanced electron spin rotation in CdS quantum dots

Yasuaki Masumoto[*], **Hikaru Umino, Jianhui Sun, and Eri Suzumura**

We studied the spin rotation of electrons in CdS quantum dots (QDs) and CdS QDs with charge acceptors by means of time-resolved Faraday rotation (TRFR) at room temperature. The electron spin rotation gave an oscillatory component in TRFR signal and the oscillation frequency proportional to magnetic field gave the *g*-factor of electrons 1.965±0.006. Non-oscillatory component comes from population of excitons and showed additional decay in CdS QDs with hole acceptor. Electron spin rotation signal was largely enhanced and lasted for spin coherence time of $T_2^* = 450$ ps in CdS QDs tethered to TiO$_2$ electron acceptor, where the spin initialization was triggered by the positive trion transition. These results give clear evidence that the electron spin rotation signal in QDs can be enhanced by transient *p*-doping.

1 Introduction

Spins of both localized electrons in semiconductors and confined electrons in semiconductor quantum dots (QDs) have long coherence time. They are candidates of solid-state qubits for quantum information processing. It is desirable for electron spins to be coherent for long time at room temperature. Time-resolved Faraday rotation (TRFR) was used to measure the excitonic population and spin rotation of electrons in CdSe and CdS QDs under the transverse magnetic field at room temperature [1,2]. Low natural abundance of nuclear spins and small hyperfine constant of Cd make spin coherence time of electrons in CdSe and CdS QDs long. Gupta *et al.* considered spins of photoexcited electrons are rotating in CdSe QDs [1]. On the other hand, Feng *et al.* considered spins of residual electrons are rotating in nominally undoped CdS QDs and that residual electrons come from oleic acid capping the surface of QDs [2]. But, initialization mechanism of electron spins is not clear. To clarify the electron source and spin initialization mechanism, TRFR study of intentionally doped QDs is favorable.

So far chemically grown QDs were intentionally doped by the formation of the shell in the type-II alignment. In photo-excited type-II CdTe/CdSe core-shell QDs, He et al. uniquely reported that electron-hole separation in QDs suppressed the electron-hole exchange interaction and lengthened the spin relaxation time of holes [3]. But valid comparison of type-II CdTe/CdSe core-shell QDs with type-I CdTe/CdSe core-shell QDs and bare CdTe QDs requires the same growth process of three kinds of samples. Comparison of p-type QDs with undoped QDs grown by the same process is preferable.

Efficient acceptor of electrons are known by the study of the QDs-sensitized solar cells of the Grätzel type. Fast and efficient electron transfer from QDs to the porous TiO$_2$ film was observed by means of time-resolved pump-probe spectroscopy and time-correlated single photon counting of luminescence [4–6], when QDs are tethered to TiO$_2$ through molecular linkers. Hole acceptor molecules for QDs are known, too [7,8]. By assembling QDs donor and acceptor of electrons (holes), we can extract electrons (holes) from photo-excited QDs and have transient *p*-type (*n*-type) QDs, assuming the remained holes (electrons) have long lifetime comparable to the repetition period of the excitation pulses. We can obtain undoped, p-type and n-type QDs from the same QDs stock solution.

Electrons, holes and excitons in semiconductor have different *g*-factors and different spin rotation frequencies in the magnetic field. In this work, we observed electron spin rotation in free-standing CdS QDs, CdS QDs tethered to electron acceptor and CdS QDs surrounded by hole acceptor by means of TRFR. Electron spin rotation in CdS QDs tethered to electron acceptor was prolonged and highly enhanced. Excitonic population and spin rotation of electrons showed additional dumping in CdS QDs surrounded by hole acceptor.

2 Experimental

2.1 Synthesis of colloidal CdS quantum dots

The colloidal CdS QDs were synthesized following the method reported by Peng *et al.* [9]. First, sulfide precursor was prepared by mixing 38.4 mg sulfur powder and 6 ml of 1-octadecene (ODE). The mixture were heated to 60 °C under stirring. Then, a mixture of 307.2 mg cadmium oxide (CdO), 2.24 ml oleic acid (OA), and 28.56 ml ODE were loaded in the three-necked flask. The mixture was degassed and then

Institute of Physics, University of Tsukuba, Tsukuba 305-8571, Japan E-mail: masumoto@physics.px.tsukuba.ac.jp; Tel: +81-29-853-4248.

was heated at the temperature of 100 °C for 1 hour. After that, the flask was purged with argon and was heated up to the temperature of 270 °C. At the temperature of 270 °C, the prepared sulfide precursor was swiftly injected into the three-necked flask for the growth of CdS QDs. After the growth, the flask was cooled down to room temperature. The CdS QDs solution was loaded in the centrifuge tubes with excess amount of acetone and was centrifuged at rotation speed of 8000 rpm. The yellow solid was redissolved in hexane. A few ml of acetone was dropwise into the solution and the solution was then centrifuged at a rotation speed of at 2000-4000 rpm. The left yellow CdS QDs solids were redissolved in toluene for storage.

2.2 CdS QD-MPA-TiO$_2$ and CdS QD-TPD suspensions for spectroscopic measurements

Colloidal amorphous TiO$_2$ particles 20 nm in diameter were made from titanium isopropoxide in the same way as reported in the reference[4,11]. By adding solution of 3-mercaptopropionic acid (MPA, HS-(CH$_2$)$_2$-COOH) to suspension of TiO$_2$ particles, MPA-capped TiO$_2$ particles having the thiol group outside are made as reported in the reference[5]. Further, functionalized TiO$_2$ particles were mixed with CdS QDs in toluene. As a result, CdS QDs are tethered to TiO$_2$ particles through the thiol group and the carboxy group of linker molecules MPA, and linked CdS QD-MPA-TiO$_2$ suspension was obtained. Suspension of CdS QD-TPD was obtained by adding N,N'-Bis(3-methylphenyl)-N,N'-bis(phenyl)benzidine (TPD) to CdS QDs solution in toluene.

2.3 Time-resolved Faraday rotation spectroscopy

Three kinds of samples, CdS QD, CdS QD-MPA-TiO$_2$ and CdS QD-TPD, in cuvettes 1 mm thick were placed at the center of pole pieces of the electromagnet for the TRFR measurement at room temperature. The 225 fs laser pulses were generated every 4 μs by a 250 kHz Ti:sapphire regenerative amplifier. The center wavelength and the band width is 800 nm and 20 nm, respectively. Their second harmonic pulses covering the absorption edge of the CdS QDs were used as pump and probe pulses. The polarization of pump pulses was modulated by a 41 kHz photoelastic modulator (PEM) and was changed to right or left circular polarization alternatively. The linear polarization axis of the probe was rotated by 45 degrees by a half-wave plate. These pump and probe beams were focused on the sample in the transverse magnetic field geometry. The probe pulses passing through the sample were divided into two cross-linearly polarized components by a Rochon prism and two components were detected by balanced photodiodes. The differential signal from the detector was amplified by a

lock-in amplifier at the the modulation frequency of PEM and its output was amplified again by the second lock-in amplifier at the mechanical chopping frequency of 210 Hz.
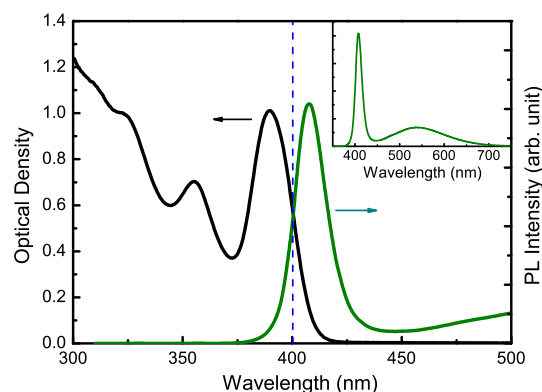
3 Results and discussion

Fig. 1 Absorption and photoluminescence (PL) spectra of CdS QDs 3.0 nm in average diameter in toluene shown by a black line and a green line, respectively. The inset shows the PL spectrum extending to longer wavelength. The pump and probe photon energies in the time-resolved Faraday rotation experiment are degenerate and are shown by a vertical blue dashed line.

The absorption and photoluminescence (PL) spectrum of CdS QDs in toluene are shown in Fig.1. The lowest energy peak in the absorption spectrum is located at 389 nm which gives the average diameter of 3.0 nm based on the relationship between the diameter of QDs and the absorption peak wavelength in the bibliography[10]. Photoluminescence spectrum peaks at 408 nm and the Stokes shift, 19 nm, suggests the exciton localization in QDs. A broad luminescence spectrum peaked at 540 nm comes from recombination between electrons and holes trapped separately at the surface of CdS QDs[11]. Time-correlated single photon counting measurement of CdS QDs showed the excitonic luminescence decays multiexponentially and tails off at 3 μs. Luminescence around 540 nm decays multiexponentially and tails off at 5 μs. Electron-hole separated state is kept for long time.

The lowest unoccupied molecular orbital (LUMO) levels and the highest occupied molecular orbital (HOMO) levels of CdS QDs 3.0 nm in diameter, amorphous TiO$_2$ particles and TPD molecules are shown in Fig.2. Cyclic voltammetry and optical absorption measurements gave CdS QDs 3.0 nm in diameter the electron affinity of -3.35 eV and ionization potential of -6.6 eV. They gave amorphous TiO$_2$ particles
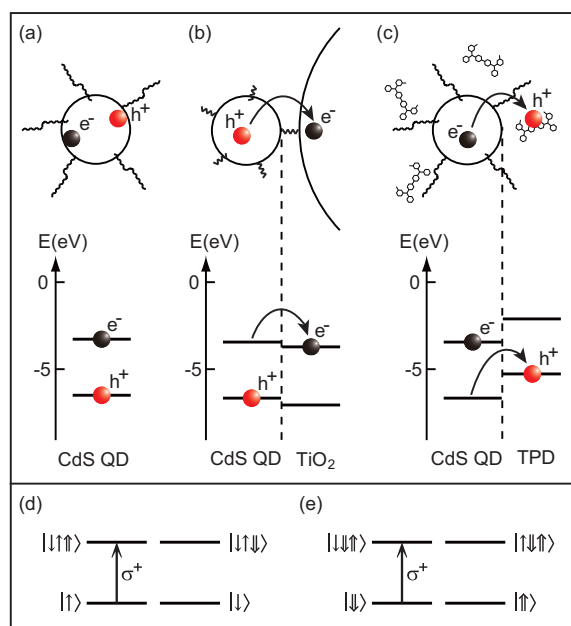
Fig. 2 Top row: Drawings of (a) a CdS QD partially capped by oleic acid, (b) a CdS QD tethered to a TiO$_2$ nanoparticle through 3-mercaptopropionic acid (MPA), and (c) a CdS QD partially capped by oleic acid with TPD molecules. Middle row: Schematic energy level diagram of the LUMO and HOMO levels of CdS QDs, amorphous TiO$_2$ and TPD. Possible electron (hole) transfer from QDs donor to TiO$_2$ (TPD) acceptor is shown by an arrow. Bottom row: Spin initialization by the trion transition. Electron spin is denoted by $|\downarrow\rangle$ or $|\uparrow\rangle$, and hole spin is denoted by $|\Downarrow\rangle$ or $|\Uparrow\rangle$. Right circular polarization is denoted by σ^+.

Fig. 3 Time-resolved Faraday rotation (TRFR) signal (solid squares) for (a) CdS QD under B=0.539 T, (b) CdS QDs-MPA-TiO$_2$ under B=0.528 T and (c) CdS QDs-TPD under B=0.539 T. Red curves are fitting by (a) 5.20exp($-t$/4510[ps])+2.40exp($-t$/404[ps])cos($2\pi t$/69.1[ps]-0.67π), (b) 3.45exp($-t$/1110[ps])+7.69exp($-t$/450[ps]) cos($2\pi t$/72.7[ps]-0.68π) and (c) 3.75exp($-t$/341[ps]) + 1.22exp($-t$/257[ps])cos($2\pi t$/66.1[ps]-0.73π) and blue curves represent the nonoscillatory component.

the electron affinity of -3.95 eV and ionization potential of -7.15 eV. It is known that TPD has the electron affinity of -2.1 eV and ionization potential of -5.4eV [7]. We can expect electron transfer from CdS QDs to TiO$_2$ particles and hole transfer from CdS QDs to TPD, as schematically shown in Fig.2. Excitonic luminescence quenching was observed in CdS QD-MPA-TiO$_2$, while partial excitonic luminescence quenching was observed in CdS QD-TPD. Luminescence quenching was observed around 540 nm in CdS QD-MPA-TiO$_2$, too, as was reported by the reference [11]. Reflecting electron transfer from CdS QDs donor to TiO$_2$ acceptor, electron-hole separated state is preserved for long time. Its lifetime was measured to be 2.6 μs by transient absorption [11].

The TRFR signals of three kinds of samples have the different amplitudes of the oscillatory component and the nonoscillatory component, as shown in Fig.3. Note that the vertical scale interval means the same intensity of the TRFR signal. The TRFR signal of CdS QD-MPA-TiO$_2$ has largely enhanced oscillatory component and that of CdS QD-TPD has decaying non-oscillatory component. All the TRFR sig-
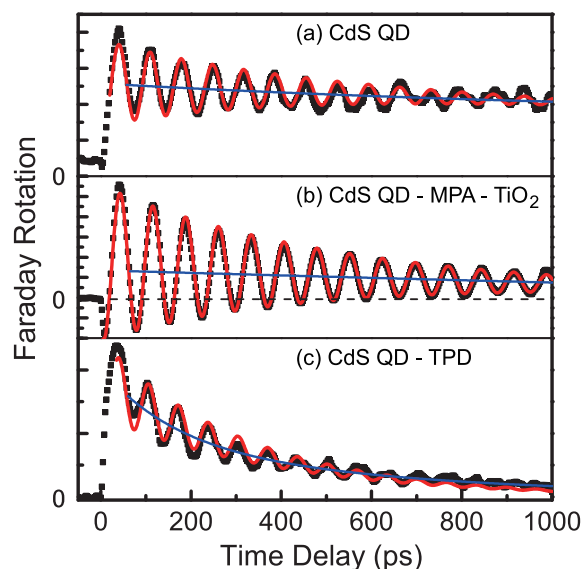
nals are written in common by the sum of the dumped oscillation coming from Larmor precession of the carrier spins and the single exponential decay. The time constant of the exponential decay means the dephasing time of the spin ensemble. The TRFR signal $\theta_F(t)$ was fitted by the equation, $\theta_F(t) = a_1\exp(-t/\tau) + a_2\exp(-t/T_2^*)\cos(2\pi\nu_L t + \phi)$, where a_1, a_2, τ, T_2^*, ν_L and ϕ are fitting parameters. Parameters a_1, τ and a_2 denote an amplitude of the nonoscillatory component, a decay constant of the nonoscillatory component and an amplitude of the oscillatory component, respectively. Parameters ν_L and T_2^* correspond to the Larmor frequency and the dephasing time of the spin ensemble, respectively. A parameter ϕ is the initial phase. Comparing the fitting parameters, we note T_2^* is longest for CdS QD-MPA-TiO$_2$ and that T_2^* is shortest for CdS QD-TPD. The amplitude of oscillatory component is largest for CdS QD-MPA-TiO$_2$ and smallest for CdS QD-TPD.

Magnetic field dependence of the Larmor frequency ν_L gives the g-factor, $g = h\nu_L/\mu_B B$, where μ_B is the Bohr magneton and B is the magnetic field. As is shown in Figs.4(a) and 4(c), ν_L is propotional to B for CdS QDs-MPA-TiO$_2$, and the slope gives the g-factor. The similar linear dependence held for CdS QD and CdS QD-TPD. The g-factors obtained are $g = 1.965\pm0.006$, 1.95 ± 0.05 and 1.91 ± 0.06 for CdS QD,
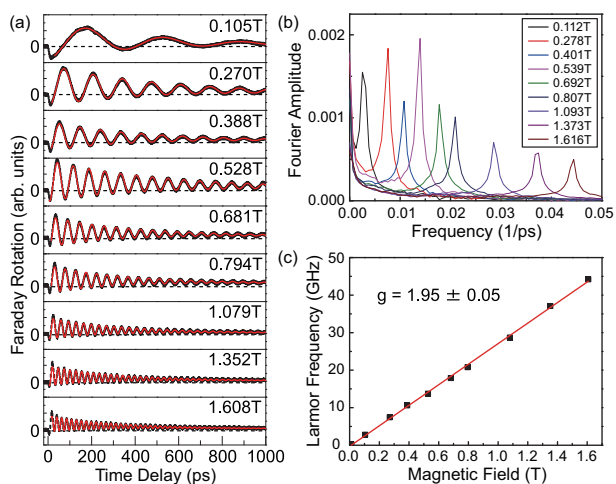
Fig. 4 (a) The TRFR signals (solid squares) in CdS QD-MPA-TiO$_2$ under transverse magnetic field. Red curves are fittings by a single exponential decay plus a dumped oscillation. (b) Fourier transform of the TRFR signals. (c) Larmor frequency (solid squares) as a function of transverse magnetic field. A red linear fitting gives the g-factor of 1.95±0.05.

CdS QD-MPA-TiO$_2$ and CdS QD-TPD, respectively. These g-factors agree with each other within the margin of errors. Therefore we took $g = 1.965\pm0.006$ having the smallest error. Fourier transform of the TRFR signals shown in Fig.4(b) consists of a single frequency peak. Thus the oscillation signal comes from one of an electron, a hole and an exciton.

In hexagonal CdS crystal having c-axis, $g_{e\perp}$=1.72±0.1 and $g_{e\parallel}$=1.78±0.05 are known [12], where $g_{e\perp}$ and $g_{e\parallel}$ are electron g-factors for $B\perp c$ and $B\parallel c$, respectively. Therefore g-factor of electron in CdS crystal is isotropic within the experimental error and is denoted by g_e. On the other hand, the g-factor of hole in hexagonal CdS crystal are highly anisotropic and $g_{h\perp}$=0 and $g_{h\parallel}$=1.15±0.05 are known [12,13]. When the angle between B and the c-axis is θ, the g-factor of hole is given by $g_{h\parallel}\cos\theta$ [13]. The bright A-exciton g-factor is given by g_e, $g_e - g_{h\parallel}$ and $g_e - g_{h\parallel}\cos\theta$ for $B\perp c$, $B\parallel c$ and $\angle(B,c) = \theta$, respectively. If the c-axis is oriented randomly to the magnetic field like CdS QDs colloids, the g-factors of hole and exciton are distributed from 0 to 1.15 and from g_e-1.15 to g_e, respectively. In this case, we can not observe long-lasting oscillatory signal of the Faraday rotation of spins for holes and excitons in hexagonal CdS QDs, but can observe fast dumping of oscillatory signal within the inverse of broadening of Larmor freuency, $2\pi\hbar/1.15\mu_B B$. At B=0.5 T, it is 124 ps. We can exclude spin rotation of holes and excitons to explain the oscillatory component in the TRFR signal.

Because the electron g-factor alone is isotropic, the electron spin rotation in CdS QDs gives the long-lasting oscilla-

tory component in the TRFR signal. The electron g-factor in QDs is evaluated by the modified Roth formula, $g = g_0 - (2/3)E_P\Delta_{so}/[(E_g + E_c + \Delta_{so})(E_g + E_c)]$, where $g_0 = 2$ is the g-factor of the free electron, E_P is the Kane energy parameter, Δ_{so} is the spin-orbit splitting of the valence band, E_g is the band gap energy of the bulk semiconductor, and E_c is the electron confinement energy [14]. Therefore the electron g-factor in CdS QDs is considered to approach to g_0=2 with the decrease in size, because of the confinement-induced energy shift of the electron energy in the conduction band. Using the CdS parameters, E_g=2.40 eV, E_P=21.0 eV and Δ_{so}=0.062eV,[15] and the CdS QD parameter, $E_g + E_c \sim 3.185$ eV, we can evaluate the confinement-induced increase of the electron g-factor to be 0.063. The estimate is smaller than the measured increase of 0.2, but the g-factor of 1.965±0.006 is regarded as the g-factor of electron in CdS QDs 3.0 nm in diameter. Similar electron g-factor of 1.93 was reported for CdS QDs 5.6 nm in diameter [2].

Circularly polarized laser pulse excites population of excitons in CdS QDs having no residual electrons and holes and produces the nonoscillatory component in the TRFR signal [2]. However, considerable portion of both electrons and holes remains in CdS QDs at 4μs after the preceding pulses excite the electron-hole pairs, because lifetime of electron-hole separated state was as long as 2.6μs [11]. In the transverse magnetic field, electron spin rotation starts after right (left) circularly polarized laser pulse excites negative trion composed of a hole and two spin-singlet electrons $|\downarrow\uparrow\Downarrow\rangle$ ($|\downarrow\uparrow\Uparrow\rangle$) from a residual electron $|\downarrow\rangle$ ($|\uparrow\rangle$) as is shown in Fig.2(d), because electron spin population at the $|\uparrow\rangle$ ($|\downarrow\rangle$) state becomes larger than that at the $|\downarrow\rangle$ ($|\uparrow\rangle$) state [16]. From a residual hole $|\Downarrow\rangle$ ($|\Uparrow\rangle$), right (left) circularly polarized laser pulse excites the positive trion composed of two spin-singlet holes and an electron $|\downarrow\Uparrow\Downarrow\rangle$ ($|\uparrow\Uparrow\Downarrow\rangle$) as is shown in Fig.2(e), and positive trion spin, that is equivalent to electron spin, starts rotating in the transverse magnetic field.

In CdS QD-MPA-TiO$_2$ composite, electron transfer from QDs to TiO$_2$ takes place efficiently at the time constant of 1110 ps in consistent with electron transfer rate reported for CdSe QD-MPA-TiO$_2$ having the similar LUMO energy difference, 0.6 eV, between donor and acceptor [4]. Reflecting the transfer time of electrons, non-oscillatry component coming from population of excitons decays at the time constant of 1110 ps. Then considerable portion of holes remains in QDs at 4 μs after the preceding pulses excites the trion composed of an electron and 2 holes, because lifetime of electron-hole separated state was as long as 2.6 μs [11]. The positive trion transition from a residual hole shown in Fig.2(e) initializes the spin rotation of electron. Transient p-doping of QDs increased the spin rotation signal of electrons by 3 times and clarified spin initialization mechanism of the positive trion transition. In CdS QD-TPD, photoexcited holes are transfered from QDs to

TPD and electrons are remained in QDs. The spin initialization by the negative trion transition shown in Fig.2(d) works in CdS QD-TPD. Population of excitons decays at the time constant of 341 ps reflecting the transfer rate of holes.

The dephasing relaxation time of T_2^* is 400 ps, 450 ps and 260 ps in CdS QD, CdS QD-MPA-TiO$_2$ and CdS QD-TPD, respectively. The longest T_2^* was observed in CdS QD-MPA-TiO$_2$. This means electron spin relaxation is slowest in p-doped QDs, where a positive trion spin alone is rotating in QDs after the photoexcitation. Electron transfer time from QDs to TiO$_2$, 1110 ps, is longer than T_2^* of electron spin dephasing time, 450 ps, and therefore reduces T_2^* little. Low natural abundance of nuclear spins [^{111}Cd (I=1/2, 12.80%), ^{113}Cd (I=1/2, 12.22%), ^{33}S (I=3/2, 0.75%)] and small hyperfine constant of Cd (I=1/2) in CdSe and CdS QDs make spin coherence time of electrons as long as T_2^*= 450 ps at room temperature.

4 Conclusions

In conclusion, we applied TRFR measurement to CdS QDs and CdS QDs with charge acceptors, TiO$_2$ nanoparticles and TPD molecules, at room temperature. We found that TRFR signal is the sum of the oscillatory signal coming from the rotation of electron spins and non-oscillatory signal coming from the excitonic population in CdS QDs. The g-factor was determined to be g = 1.965±0.006 from the oscillation frequency proportional to magnetic field, and the dephasing relaxation time of T_2^* was about 450 ps for CdS QDs tethered to TiO$_2$. Non-oscillatory component comes from population of excitons and showed additional decay in CdS QDs with hole acceptor. Electron spin rotation signal is largely enhanced in CdS QDs tethered to TiO$_2$. The spin initialization was triggered by the positive trion transition. Transient p-doping of QDs increased the electron spin rotation signal.

Acknowledgement

References

1 Gupta, J. A.; Awschalom, D. D.; Efros, Al. L.; Rodina, A. V. *Phys. Rev. B* 2002, **66**, 125307.

2 Feng, D. H.; Li, X.; Jia, T. Q.; Pan, X. Q.; Sun, Z. R. and Xu, Z. Z. *Appl. Phys. Lett.* 2012, **100**, 122406.

3 He, J.; Zhong, H. and Scholes, G. D. *Phys. Rev. Lett.* 2010, **105**, 046601.

4 Robel, I.; Subramanian, V.; Kuno, M. and Kamat, P. V. *J. Am. Chem. Soc.* 2006, **128**, 2385.

5 Hyun, B.-R.; Zhong, Yu-Wu.; Bartnik, A. C.; Sun, L.; Abruña, H. D.; Wise, F. W.; Goodreau, J. D.; Matthews, J. R.; Leslie, T. M. and Borrelli, N. F. *ACS Nano* 2008, **2**, 2206.

6 Masumoto, Y.; Takagi, H.; Umino, H. and Suzumura, E. F. *Appl. Phys. Lett.* 2012, **100**, 252106.

7 Coe, S.; Woo, W.-K.; Bawendi, M. and Bulović, V. *Nature* 2002, **420**, 800.

8 Jing, P.; Yuan, X.; Ji, W.; Ikezawa, M.; Liu, X.; Zhang, L.; Zhao, J. and Masumoto, Y. *Appl. Phys. Lett.* 2011, **99**, 093106.

9 Yu, W. W. and Peng, X. *Angew. Chem. Int. Ed.* 2002, **41**, 2368.

10 Yu, W. W.; Qu, L.; Guo, W. and Peng, X. *Chem. Mater.* 2003, **15**, 2854.

11 Dibbell, R. S. and Watson, D. F. *J. Phys. Chem. C.* 2009, **113**, 3139.

12 Hopfield, J. J. and Thomas, D. G. *Phys. Rev.* 1961, **122**, 35.

13 Thomas, D. G. and Hopfield, J. J. *Phys. Rev.* 1962, **128**, 2135.

14 Kiselev, A.A.; Ivchenko, E. L.; Rössler, U. *Phys. Rev. B* 1998, **58**, 16353.

15 Ithurria, S.; Tessier, M. D.; Mahler, B.; Lobo, R. P. S. M.; Dubertret, B. and Efros, Al. L. *Nat. Mater.* 2011, **10**, 936.

16 Greilich, A.; Oulton, R.; Zhukov, E. A.; Yugova, I. A.; Yakovlev, D. R.; Bayer, M.; Shabaev, A.; Efros, Al. L.; Merkulov, I. A.; Stavarache, V.; Reuter, D. and Wieck, A. *Phys. Rev. Lett.* 2006, **96**, 227401.